JOURNAL OF CHEMICAL INFORMATION AND MODELING

Article

pubs.acs.org/jcim

Identification of Novel Phosphodiesterase-4D Inhibitors Prescreened by Molecular Dynamics-Augmented Modeling and Validated by Bioassay

Zhe Li,[†,⊥] Ying-Hong Cai,[†,⊥] Yuen-Kit Cheng,[‡] Xiao Lu,[†] Yong-Xian Shao,[†] Xingshu Li,[†] Ming Liu,[†] Peiqing Liu,[†] and Hai-Bin Luo*[,†]

[†]School of Pharmaceutical Sciences, Sun Yat-Sen University, Guangzhou 510006, PR China

[‡]Department of Chemistry, Hong Kong Baptist University, Kowloon, Hong Kong

Supporting Information

ABSTRACT: Phosphodiesterase-4D (PDE4D) has been proved to be a potential therapeutic target against strokes. In the present study, a procedure of integrating pharmacophore, molecular docking, molecular dynamics (MD) simulations, binding free energy calculations, and finally validation with bioassay was developed and described to search for novel PDE4D inhibitors from the SPECS database. Among the 29 compounds selected by our MD-augmented strategy, 15 hits were found with IC_{50} between 1.9 and 50 μM (a hit rate of 52%) and 6 potent hits showed IC_{50} less than 10 μM, which suggested that MD simulations can explore the intermolecular interactions of PDE4D−inhibitor complexes more precisely and thus significantly enhanced the hit rate of this screening. The effective and efficient integrated procedures described in this study could be readily applied to screening studies toward other drug targets.

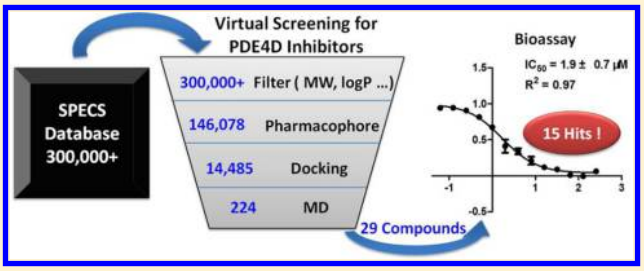

1. INTRODUCTION

Intracellular cyclic adenosine monophosphate (cAMP), which is one of the important second messengers involved in signaling pathways, plays crucial roles in regulating many physiological processes, such as inflammation, cell growth, and sensory signaling due to its ubiquitous distribution. Evidence has shown that the increase of cAMP level suppresses the activity of a variety of inflammatory cells, such as macrophages, T cells, and neutrophils.[1,2] The concentration of cAMP is controlled by the cyclic nucleotide phosphodiesterase (PDE) which comprises a group of enzymes that degrade the second messengers cAMP and cGMP (cyclic guanosine monophosphate). The PDE superfamily of enzymes is classified into 11 families, and different PDEs have different substrate specificities. Inhibition of different PDEs can cause different biological functions due to their unique tissue distribution and functional properties.[3−10] As a cAMP-specific enzyme, PDE4 is mainly distributed in inflammatory and immune cells and has been proved to be a therapeutic target for several diseases, such as asthma and chronic obstructive pulmonary disease (COPD).[11−16] Our recent research also revealed that resveratrol can ameliorate aging-related metabolic phenotypes by inhibiting cAMP-specific PDE3 and PDE4,[17] and thus PDE4 may serve as a potential antiaging target.

In 2003, PDE4D has been identified as a novel stroke-related gene by using genomewide association screen.[18] Inspired by this work, great attention including experimental and theoretical efforts has been paid to investigate the relationships between PDE4D and stroke,[19−23] which is one of the top three leading reasons of death worldwide. Thus, the discovery and development of novel PDE4D inhibitors could reduce stroke risk through the inhibition of PDE4D.[22]

The purpose of the current study is to provide a molecular dynamics (MD)-augmented strategy for the screening of PDE4D inhibitors against stroke. Herein, a screening study on the SPECS database (http://www.specs.net) has been performed through an MD-augmented protocol consisted of several approaches (Figure 1), such as pharmacophore, molecular docking, MD simulations, binding free energy (ΔG_{pred}) calculations, and bioassay, in order to identify potent and novel PDE4D inhibitors. After 8 ns MD simulations for 224 PDE4D−inhibitor complexes, 29 compounds with relatively negative theoretical ΔG_{pred} and appropriate binding patterns were retained and ordered for bioassay. Among the 29 compounds selected by our strategy, 15 hits were found with IC_{50} values ranging from 1.9 to 50 μM (a hit rate of 52%), which suggested this combined method is a promising and effective approach to discover new PDE4D inhibitors which may reduce stroke risks and could be applied in screenings toward other drug targets. Taken together, this work provides new hit molecules and structural clues for the discovery of PDE4D inhibitors with desirable biological activities.

Received: January 28, 2013
Published: March 21, 2013

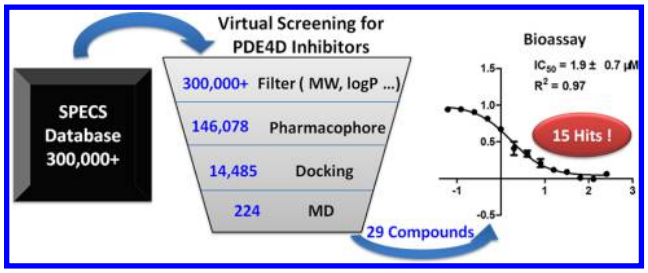

Figure 1. Strategy for the molecular dynamics-augmented virtual screening of PDE4D inhibitors.

2. MATERIALS AND METHODS

2.1. Database Preparation. In view of the structural diversity and availability at the time of study, among the numerous commercial and academic compound databases, the SPECS database was selected for the screening purpose. The SPECS database with over 300 000 compounds was prefiltered by our rules, which were quite similar to well-known Lipinski's Rule of Five except molecular_weight ≤ 600 in view of the filter rules of Molecular Operating Environment (MOE 2008.10)[24,25] software, in order to obtain the preliminary database **Database0** using an *in-house* program. For each compound, a set of physical and biological properties were predicted and used to assess its drug-likeness profile. Conformations (250) of each molecule were generated through MOE 2008.10 by using the conformation import method for each molecule (Note that the conformation import method in MOE contains filter rules, molecules with the following properties were removed by default: molecular weight > 600, logP < −4, logP > 8, H-bond donors + acceptors > 12, rotatable bonds > 7, single bond chain length > 6, chiral centers > 4, unconstrainted chiral centers > 3, transition metals > 8 rings, and d-hybrids). After filtering, the database size was significantly reduced from over 300 000 structures to 146 078.

2.2. Pharmacophore Model Generation and Database Screening. Pharmacophore models were first generated by using software MOE 2008.10. Here five high-resolution crystal structures of PDE4D from Protein Data Bank (PDB code: 3G4I, 1.90 Å, 3G4K, 1.95 Å, 1XOQ, 1.83 Å, 1XOM, 1.55 Å, and 1XON, 1.71 Å)[26,27] were used to construct pharmacophore models. The five crystal structures were first superimposed by residues, and as a result the ligands in the structures were also superimposed. On the basis of the superimposed ligands, consensus pharmacophore features was generated by MOE software, and only the features mapping all the five ligands were kept in the pharmacophore model. Considering the similarity between some features, the aromatic center feature was changed to a unified Aro|PiR (aromatic center or Pi ring center) feature, and the hydrophobic centroid feature was changed to Hyd|Aro (hydrophobic centroid or aromatic center) feature. The excluded volume was then generated by the protein residues near the binding-site pocket. Due to the similar volumes of the binding-site pockets in the five crystal structures, only 1XOQ was used in the excluded volume generation.

After pharmacophore model was generated, it is crucial to test if a model can distinguish active compounds from random compounds against a special target. Herein, a decoy set, which contained 197 active inhibitors from the Binding Database[28] (http://www.bindingdb.org) and 855 inactive compounds randomly selected from the DUD database,[29] was constructed to validate the reliability of the derived pharmacophore model via an evaluation of goodness of hit (GH) test.[30−32] The GH test can be used to enhance the confidence of statistical significance when screening a compound database. The conformation generation method for the decoy set was the same as the one used for the SPECS database. The pharmacophore model was then modified several times based on the GH test score to improve its predictive efficacy. The radius of each pharmacophore feature spheres was increased or decreased. Finally, a pharmacophore model was generated with its GH test score >0.5, which means that it is a good model for screening.

After that, all the compounds in **Database0** were searched to find compounds matching all the features of the derived pharmacophore model in order to generate the initial database **Database1** for the subsequent docking screening studies.

2.3. Molecular Docking Screening. The crystal structure of PDE4D in complex with the drug roflumilast (PDB code 1XOQ) at a resolution of 1.83 Å[26] was used for the docking screening studies. The protein contains two metal ions (Mg^{2+} and Zn^{2+}), and most of the crystallographic water molecules were removed except the ones which form coordination bonds with the two metal ions. Hydrogen atoms were added with all ionizable residues protonated at a neutral pH. After the preparation of the receptor structure, a docking protocol CDOCKER[33] embedded in Accelrys Discovery Studio 2.5.5 was used for the molecular docking study. The active site of PDE4D was constructed by using roflumilast as a reference ligand. Ten random conformations were generated for each ligand. The rest of the parameters were set to the default values. From the 10 poses, we chose the optimal one in terms of both the docking scores and cluster popularity.

Before the CDOCKER screening, 30 PDE4D inhibitors (Figure S1, see the Supporting Information) were selected from the Binding Database to probe the threshold of docking scores under identical docking conditions. As a result, the average CDOCKER score of the top "−CDOCKER_INTERACTION_ENERGY" for the 30 inhibitors was 40 kcal/mol.

Thus, those compounds in **Database1** were filtered out with their CDOCKER docking scores less than the threshold of 40 kcal/mol and without an appropriate binding motif via visual inspection of the docked poses. This appropriate motif gave special emphasis to both hydrogen bond interactions occurring with Gln369 and $\pi-\pi$ stacking interactions occurring with Phe372. It is well-known that there are examples of PDE4 inhibitors that can bind to the cAMP binding site by forming one or two hydrogen bonds with Gln369 and stacking against Phe372. Additionally, the visual inspection step can help to identify compounds that exhibited unfavorable interactions with the binding site in PDE4D or compounds that adopted unrealistic conformations when docked into the binding site. This docking screening retained over 200 compounds with appropriate binding patterns and higher docking scores than 40 kcal/mol, which were selected as the intermediate database **Database2.**

After the molecular docking procedures, over 200 systems that PDE4D are in complex with the compounds in **Database2** were prepared and were submitted to subsequent MD simulations and ΔG_{pred} calculations.

2.4. MD Simulations. Molecular docking method only reflects a possibly instantaneous binding mode which may be not reasonable/stable between a ligand and a receptor. So the MD simulations method was then applied to perform further

dx.doi.org/10.1021/ci400063s | J. Chem. Inf. Model. 2013, 53, 972−981

evaluation of the binding stabilities between all the compounds in **Database2** and their receptor PDE4D.

The MD simulations were based on the docking structures, and AMBER 10.0[34] was used for all the MD simulations. The partial atomic charges of the ligands in **Database2** were calculated by Gaussian 03 program[35] by using the Hartree−Fock method with the 6-31G(d) basis set, and the Antechamber program was then used for fitting the restricted electrostatic potential (RESP) and assigning GAFF force field parameters.[36] For the protein, the AMBER ff03 force field was used. The Zn^{2+} and Mg^{2+} ions in the binding pocket were treated by the "nonbond model" method.[37] For each receptor−ligand complex, 8 Å truncated octahedral box of water were added and Na^+ ions were used to neutralize the whole system.

The simulations were performed at a neutral pH, with histidines 164 and 200 protonated at δ position (they were changed from HIS to HID) to form coordination bonds with Zn^{2+} and Mg^{2+} ions. The water molecule between Zn^{2+} and Mg^{2+} was treated as OH^- proposed by the previous study.[38] His160, which is nearest to the OH^-, can readily capture a proton and was changed to HIP (protonated His). All the bonds involving hydrogen atoms were restricted by the SHAKE algorithm,[39] and the time step was set to 2 fs. The cutoff distance was selected as 8 Å, with long-range electrostatic interactions treated with the particle mesh Ewald (PME) method. For each system, four steps of minimization were performed before the heating step. Heavy atoms in the receptor−ligand complex were restrained with degressive constraints of 500, 100, 10, and 0 kcal/(mol Å^2), respectively, whereas solvent molecules were not restrained. All the minimization steps contained 2500 cycles of steepest descent minimization, followed by 2500 cycles of conjugated gradient minimization. After minimizations, the whole system was first heated from 0 to 300 K in 50 ps using Langevin dynamics at a constant volume and, then, equilibrated for 100 ps at a constant pressure of 1 atm. A weak constraint of 10 kcal/(mol Å^2) was used to restrain all the heavy atoms in the receptor−ligand complexes during the heating and equilibration steps. Finally, periodic boundary dynamics simulations of 8 ns were carried out for the whole system with an NPT (constant composition, pressure, and temperature) ensemble at a constant pressure of 1 atm and 300 K in the production step.

2.5. MM-PBSA Estimation of Binding Free Energy ΔG_{pred}. After 8 ns MD simulations, ΔG_{pred} between PDE4D and ligands in **Database2** were calculated by the MM-PBSA (molecular mechanics Poisson−Boltzmann surface area) method.[40−43] For each system, 100 snapshots were extracted from the last 1 ns trajectory with an interval of 10 ps, which were used to calculate ΔG_{pred}.

Since the normal mode calculation of entropy is extremely time-consuming for large systems, the entropy contribution was not considered in our ΔG_{pred} calculations for the over 200 PDE4D−ligand complexes in order to reduce the computational time and save the computational cost of the MD-based screening studies. Therefore, the calculated ΔG_{pred} in the present work were not absolute ones due to the omission of the entropy contribution.

Roflumilast is a very strong PDE4D inhibitor with its IC_{50} value of 0.68 nM.[26] The ΔG_{pred} between the bound roflumilast and PDE4D predicted by the MM-PBSA method was −28.51 ± 2.65 (−25.86 to −31.16) kcal/mol. Theoretically ΔG_{exp} can be approximately estimated based on experimental IC_{50} values via $\Delta G_{exp} \approx RT \ln(IC_{50})$.[10,41] For the purpose of screening, a compound is expected to give its IC_{50} value less than 20 μM. The difference between ΔG_{exp} of roflumilast and ΔG_{exp} of a compound with its IC_{50} value of 20 μM is 6.10 kcal/mol [$RT \ln(20\,000 \times 10^{-9}/0.68 \times 10^{-9}) = 6.10$]. In order to reduce the number of false negative compounds, the threshold for ΔG_{pred} was set to a value of about −25 (−31.16 + 6.10) kcal/mol. Thus, a ligand with its ΔG_{pred} more negative than this threshold and an appropriate binding pattern via visual inspection would be retained in the finial database **Database3**. Compounds in **Database3** were purchased from SPECS and bioassayed as described below.

A ligand with its ΔG_{pred} more negative than this threshold and an appropriate binding pattern via visual inspection would be retained in the finial database **Database3**. Compounds in **Database3** were purchased from SPECS and bioassayed as described below.

2.6. Bioassay at the Molecular Level. The protocol for the expression, purification, and enzymatic assay of PDE4D has been carried out according to our previous work.[9,10,17]

Protein Expression and Purification. Recombinant plasmid pET15b-PDE4D2 (catalytic domain, 86-413) was transformed into *E. coli* strains BL21 (codonplus). The *E. coli* cells carrying recombinant plasmid grew in LB medium (containing 100 μg/mL ampicillin, 20 μg/mL chloramphenicol, and 0.4% glucose) at 37 °C until OD_{600} = 0.7. Then 0.1 mM isopropyl β-D-1-thiogalactopyranoside was used to induce PDE4D protein expression. *E. coli* cells were collected after further growing for 20 h at 15 °C. PDE4D proteins were purified mainly by nickel-nitriloacetic acid (Ni-NTA) column (Qiagen). Elution buffer with imidazole in different concentrations was used to separate PDE4D proteins, and the eluate was collected and also the concentration was estimated according to the absorbance at 280 nm (calculated by ProtParam software). The purity of the PDE4D2 protein was greater than 90% as shown by sodium dodecyl sulfate polyacrylamide gel electrophoresis (SDS-PAGE).

Enzymatic Assays. The enzymatic activities of the catalytic domains of PDE4D were measured by using cAMP as substrates. ^{3}H-cAMP was diluted with the assay buffer (50 mM Tris pH = 8.0, 10 mM $MgCl_2$, 0.5 mM dithiothreitol) to 20 000−30 000 cpm/assay. With inhibitors solution (DMSO) in different concentration added, PDE4D enzyme, which was diluted with the assay buffer previously, was added to start the enzymatic reaction. The reaction was carried out at room temperature (25 °C) for 15 min and then terminated by addition of 0.2 M $ZnSO_4$. The reaction product ^{3}H-AMP was precipitated out by 0.2 N $Ba(OH)_2$, whereas unreacted ^{3}H-cAMP remained in the supernatant. The radioactivity in the supernatant was measured in 2.5 mL Ultima Gold liquid scintillation cocktails (PerkinElmer) by a liquid scintillation counter (PerkinElmer 2910). Each measurement was repeated at least three times, and IC_{50} values were calculated by nonlinear regression. In this assay, rolipram purchased from SIGMA was used as the reference compound. All the compounds in **Database3** were subjected to bioassay.

3. RESULTS AND DISCUSSION

The schematic representation of the hit discovery strategy adopted in this study is presented in Figure 1.

3.1. Pharmacophore Modeling Results. *Quality of the Pharmacophore Model.* When generating the pharmacophore models, five crystal structures of PDE4D were superimposed and the derived pharmacophore model as shown in Figure 2

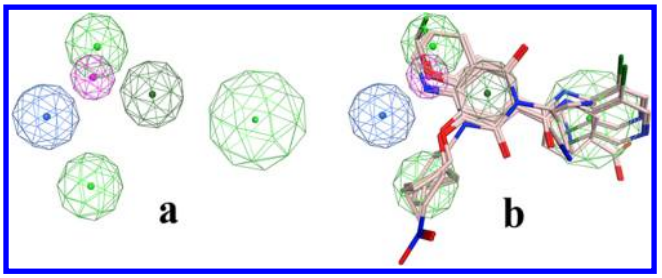

Figure 2. (a) Derived pharmacophore model for the screening of PDE4D inhibitors. The pharmacophore feature coded green represents hydrophobic centroid or aromatic center (HydlAro); dark green represents aromatic center or Pi ring center (AroIPiR); purple represents H-bond acceptor; and blue represents H-bond acceptor projection. (b) Mapping the bound ligands from the five crystal structures (PDB code 3G4I, 1.90 Å, 3G4K, 1.95 Å, 1XOQ, 1.83 Å, 1XOM, 1.55 Å, and 1XON, 1.71 Å) with the derived pharmacophore model.

Table 1. Statistical Parameters for the Screening of the Decoy Set

parameters[c]	values
(**D**) total number of molecules in database	1052 (197 + 855)
(**Ht**) total number of hit compounds in database	226
(**A**) total number of known potent compounds in database	197
(**Ha**) total number of known potent compounds in hit list	139
[(**Ha** ÷ **A**) × **100**] % ratio of known potent compounds	70.6
[(**Ha** ÷ **Ht**) × **100**] % yield of known potent compounds	61.5
(**EF**) enrichment factor[a]	3.28
(**GH**) goodness of hit test score[b]	0.57

[a]**EF** = (**HaD**/**HtA**). [b]**GH** = [**Ha**(3**A** + **Ht**)/4**HtA**][1 − (**Ht** − **Ha**)/(**D** − **A**)]. [c]Here, a hit refers to who fits the derived pharmacophore model well in the decoy set. **GH** test scores ≥0.5 and ≥0.6 indicate a good screening model and a very good screening model, respectively.

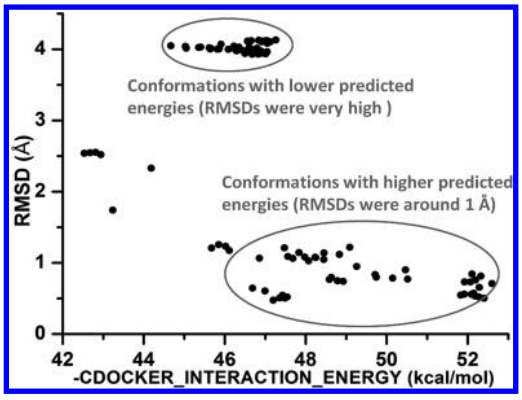

Figure 3. RMSDs between docking poses and crystal counterpart for the bound roflumilast by the CDOCKER program. 40 poses with higher docking scores gave their RMSDs below 1 Å.

was generated using the unified pharmacophore features This pharmacophore model contains three unified HydlAro features, one AroIPiR center, one H-bond acceptor, and one H-bond acceptor projection. The quality of the derived pharmacophore model was evaluated by the screening of the decoy set. Statistical parameters of this evaluation are listed in Table 1. The GH test is a benchmark for assessing the efficacy of a screening. The value of the GH test score must be >0.5 for a good screening model.[30−32] The value of GH in the present work is 0.57, which demonstrated this pharmacophore model was of high efficiency when screening compound databases.

After filtering by our rules, 146 078 compounds in **Database0** left from SPECS were subjected to the pharmacophore query. As a result, 14 485 compounds containing the pharmacophore features constituted **Database1**. This hierarchical strategy efficiently reduced the number of "non-hits" passed

Table 2. Predicted Binding Free Energies (ΔG_{pred}, kcal/mol) of the 29 Inhibitors Selected for Bioassay

no.	SPECS ID	ΔG_{pred}	std
1	AE-848/13424470	−36.99	±3.03
2	AF-399/13567299	−35.27	±3.24
3	AG-205/12549028	−33.99	±2.71
4	AG-690/11171046	−33.28	±4.42
5	AG-690/36932134	−31.91	±2.52
6	AK-968/13408004	−31.86	±2.56
7	AN-989/41261356	−30.97	±3.25
8	AN-652/43161950	−30.84	±3.17
9	AK-968/12101084	−30.75	±3.46
10	AN-698/41889463	−30.12	±2.65
11	AP-263/43302414	−30.12	±3.02
12	AK-968/40709175	−29.74	±3.82
13	AN-652/43161930	−29.18	±2.48
14	AO-080/41821182	−28.95	±3.05
15	AN-652/42999091	−28.86	±3.42
16	AN-652/43024821	−28.53	±2.98
17	AN-465/42834588	−28.18	±3.57
18	AN-979/41068914	−28.17	±3.46
19	AP-263/41599688	−28.13	±2.87
20	AN-989/40746781	−28.07	±3.05
21	AK-968/13408234	−28.02	±3.64
22	AM-807/13615173	−27.21	±2.85
23	AN-465/14952078	−26.25	±3.28
24	AN-329/41583575	−25.85	±3.41
25	AN-329/40020318	−25.80	±5.12
26	AN-652/43024779	−25.72	±3.96
27	AK-968/41922635	−25.56	±3.66
28	AN-652/40194515	−25.43	±2.46
29	AN-652/43024725	−25.39	±2.80

Table 3. IC_{50} Values (μM) of 15 PDE4D Inhibitors[a]

no.	SPECS ID	IC_{50}	std
1	AM-807/13615173	1.9	±0.7
2	AN-698/41889463	2.9	±0.5
3	AG-205/12549028	4.0	±0.8
4	AF-399/13567299	6.5	±0.5
5	AP-263/41599688	7.3	±0.2
6	AE-848/13424470	9.4	±0.2
7	AN-329/40020318	11.4	±1.1
8	AN-989/41261356	12.1	±1.2
9	AN-979/41068914	≈12.5	-
10	AK-968/13408004	13.8	±1.7
11	AN-989/40746781	17.0	±1.3
12	AK-968/41922635	30.9	±2.7
13	AO-080/41821182	≈50	-
14	AN-652/43024821	≈50	-
15	AN-652/43161930	≈50	-

[a]Rolipram serves as the reference compound for the bioassay (0.6 μM).

dx.doi.org/10.1021/ci400063s | J. Chem. Inf. Model. 2013, 53, 972−981

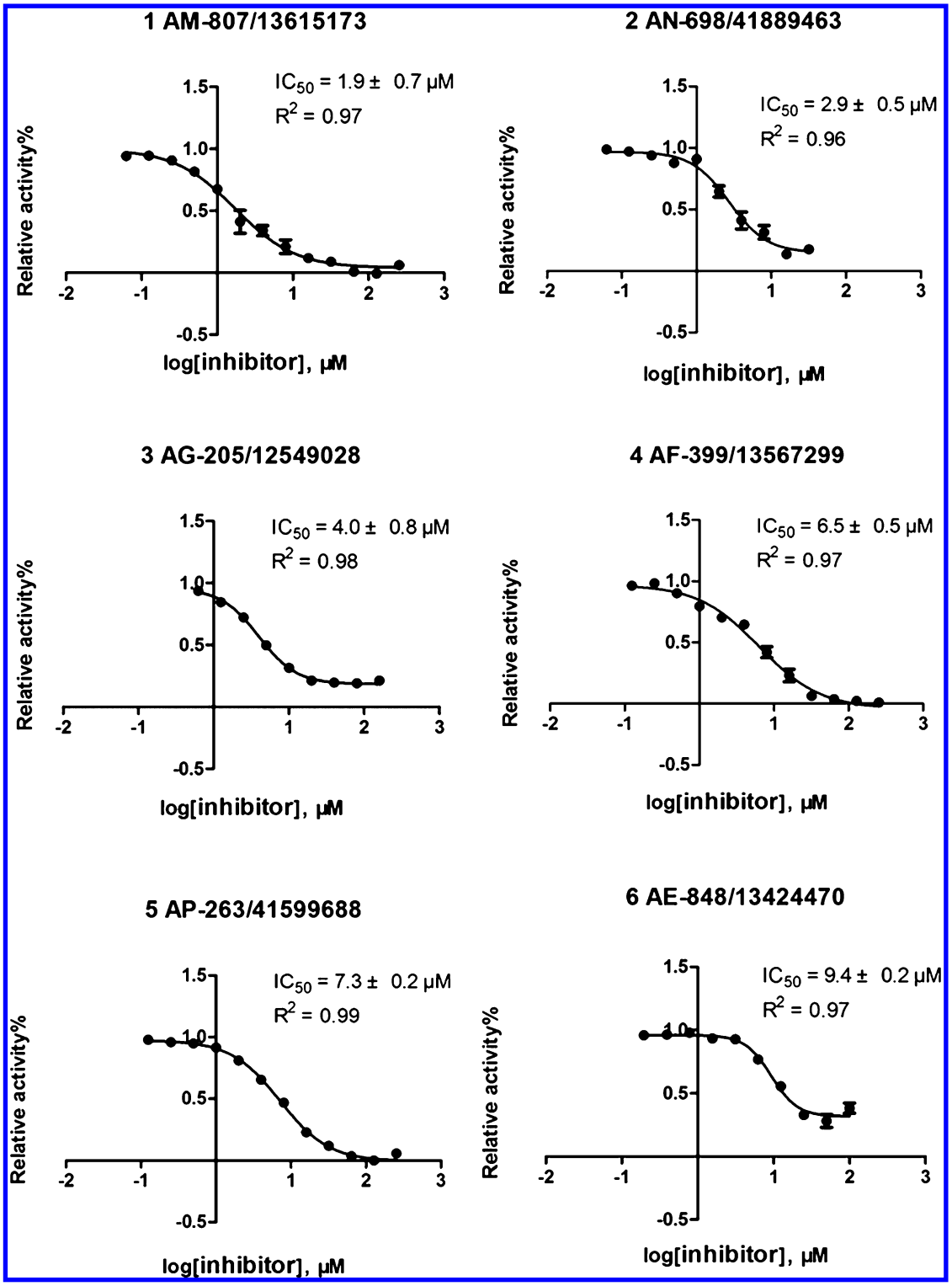

Figure 4. Inhibitory curves of six of the most potent compounds toward PDE4D.

to the molecular docking stage and consequently saved the computational cost.

3.2. Validation of the Molecular Docking Methods and Docking Results. To evaluate the reliability of the CDOCKER method, the bound roflumilast in 1XOQ was extracted from this crystal structure and redocked back to the same receptor by using of a variety of docking conditions and scoring functions. Docking is considered successful if the RMSD value of the optimum pose is smaller than a given threshold of 1.0 Å from the crystal pose after cluster analysis. The plot of RMSDs between the 100 docking poses saved and the crystal counterpart against their docking scores was shown in Figure 3. The 40 poses with the top docking scores gave their RMSDs near or below 1 Å, which suggests that CDOCKER reproduces the crystal-binding model well and is applicable to the PDE4D system.

In addition, the other two well-known and commonly used docking methods including Tripos Surflex-dock[9,44] and MOE-

dx.doi.org/10.1021/ci400063s | J. Chem. Inf. Model. 2013, 53, 972−981

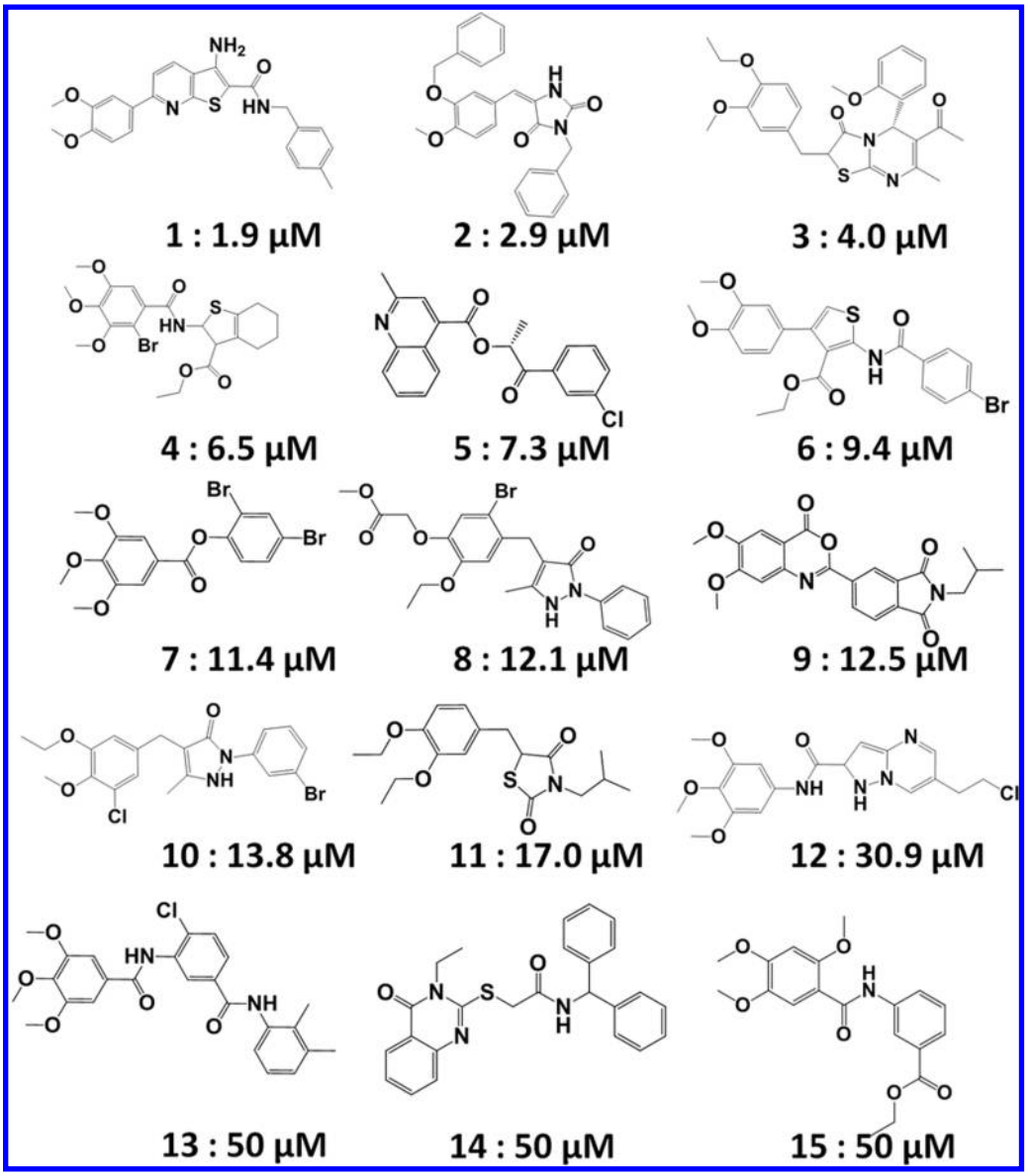

Figure 5. Chemical structures and IC_{50} values of the 15 potent inhibitors toward PDE4D.

dock[24,25] were also used for comparison. The average RMSD values of the top 40 poses for these docking approaches (CDOCKER, Suflex-dock, and MOE-dock) are 0.81, 1.30, and 1.69 Å, respectively, which demonstrated that CDOCKER was more suitable for the PDE4D system.

Thirty potent PDE4D inhibitors obtained from Binding Database were docked to the binding site pocket of 1XOQ by using CDOCKER under identical conditions. The mean value of the highest docking scores of "−CDOCKER_INTERACTION_ENERGY" for these inhibitors is 40 kcal/mol. Thus, the threshold was set to 40 kcal/mol for the screening purpose toward **Database1**. On the basis of the binding modes of these inhibitors and the threshold of 40 kcal/mol, 224 high-scoring hits were retained and constituted **Database2**.

MD Simulations and ΔG_{pred} Calculation. The crystal structure 1XOQ in complex with roflumilast was used to evaluate the reliability of our MD method. The RMSD values of the crystal structure during the MD simulations were monitored in Figure S2, and the RMSD curve was stable after 2 ns. The MD trajectories were well equilibrated and the MD parameters we chose were appropriate for the MD simulations.

Eight nanosecond MD simulations were performed for the 224 PDE4D-ligand complexes prepared from **Database2** under identical MD conditions. Most of the compounds gave stable RMSD curves during their MD simulations. In this study, 29 purchasable compounds with appropriate binding modes and ΔG_{pred} values more negative than −25 kcal/mol were selected and ordered from SPECS for PDE4D inhibitory activity assessment. The predicted ΔG_{pred} values of the 29 compounds are listed in Table 2.

Final Bioassay Validation. Herein rolipram serves as the reference compound and its IC_{50} value was 0.6 μM, which was comparable to that of 1.0 μM reported in the literature.[4] Under identical conditions, 15 of the 29 tested compounds were confirmed to be in vitro PDE4D inhibitors with their IC_{50} values $\leq$ 50 μM (Table 3). The best IC_{50} of compound **1** was 1.9 μM. Among the 15 compounds, 6 of them showed their IC_{50} values less than 10 μM, which demonstrated that they were potent PDE4 inhibitors. The inhibitory curves of the six

dx.doi.org/10.1021/ci400063s | J. Chem. Inf. Model. 2013, 53, 972−981

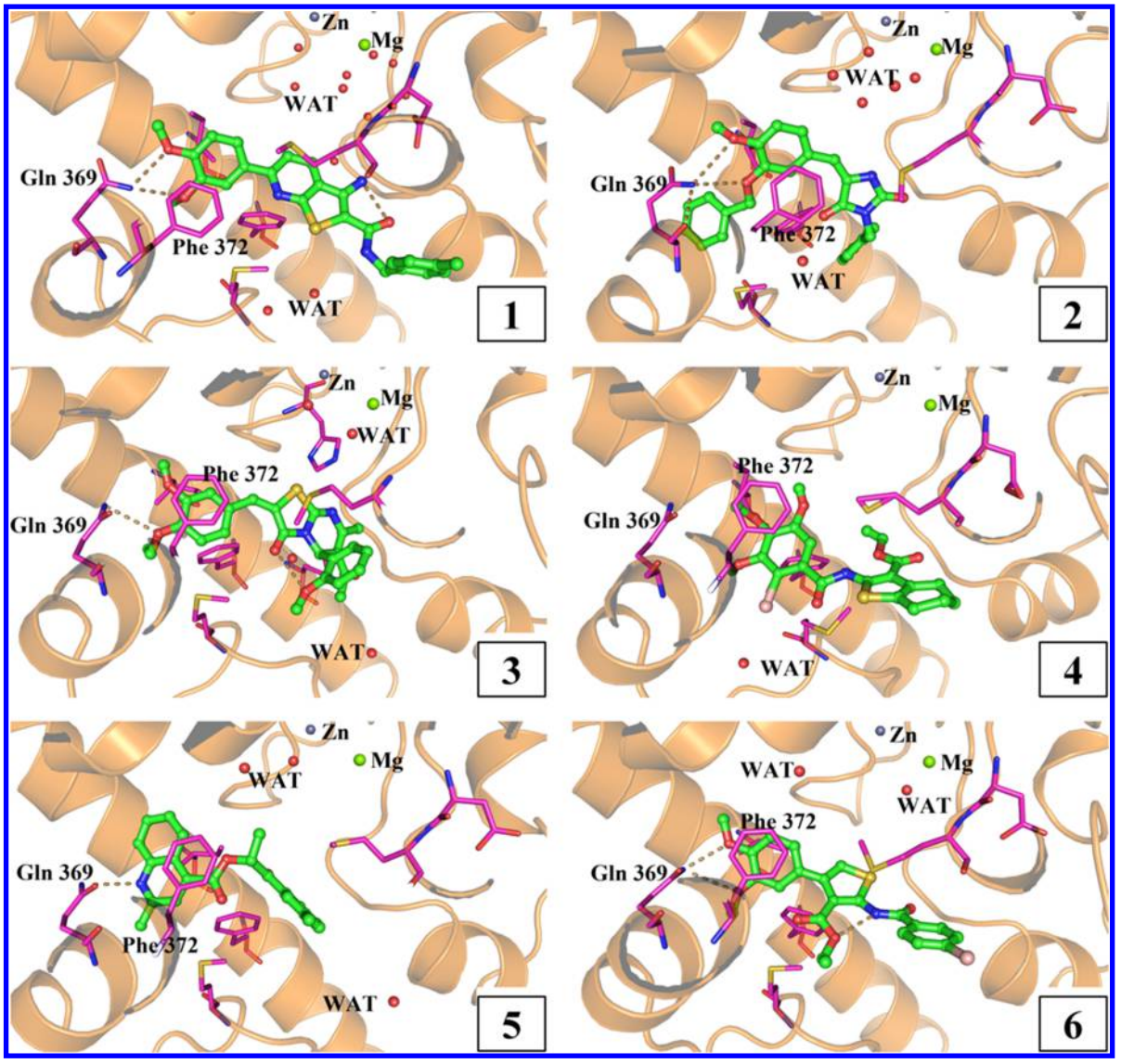

Figure 6. Binding patterns of six of the most potent compounds with PDE4D after 8 ns MD simulations. Interactions with Phe372 and Gln369 are the common features for the six compounds.

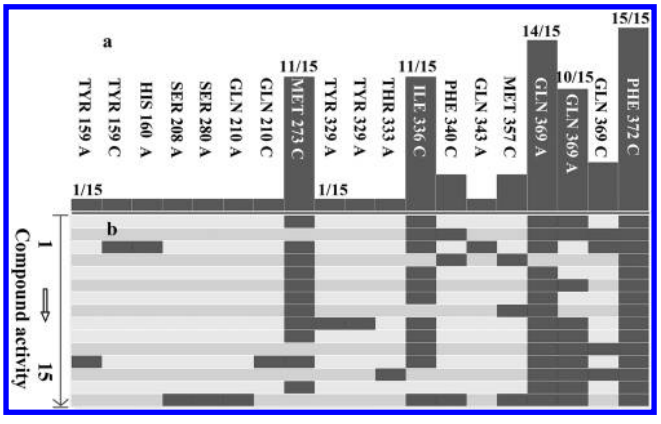

Figure 7. Protein−ligand interaction fingerprints of the 15 potent compounds. The capital letters A and C in (a) represent side chain H-bond acceptor and surface contact, respectively. (a) Population display mode of the fingerprint. (b) Barcodes display mode. The black areas represent the interactions between this receptor PDE4D and ligands.

representative compounds are shown in Figure 4, which demonstrated an unambiguous dose-dependent effect.

Augmented MD Simulations Increased the Hit Rate of Our Virtual Screening Significantly. A problem we were concerned with in the present study was whether MD simulations can improve the hit rate of the MD-based virtual screening. Since MD simulations are time-consuming and computationally costly, it would be meaningless to use them if they could not improve the hit rate significantly.

Chen et al.[23] also screened PDE4 inhibitors from the SPECS database by using both multiple pharmacophore models and molecular docking approaches. On the basis of their modeling results, 6 out of 60 compounds were found to be PDE4D inhibitors (the hit rate of their combined method is about 10%) and 4 compounds showed their IC_{50} between 1.0 and 10 μM.

With the assistance of MD simulations and ΔG_{pred} calculations, 15 out of 29 tested compounds were identified to be PDE4D inhibitors ($IC_{50} \leq 50$ μM) and 6 compounds showed their IC_{50} between 1.0 and 10 μM. As a result, the hit rate for the MD-augmented screening is 52%, which is significantly higher than that of 10% for combining

dx.doi.org/10.1021/ci400063s | J. Chem. Inf. Model. 2013, 53, 972−981

pharmacophore models and molecular docking methods in the previous virtual screening.[23] Pharmacophore models mainly consider the common features of the inhibitors, while docking methods could predict the binding orientation and binding strength between receptors and ligands. The two methods only represent the instantaneous interactions between ligands and receptors, whereas MD simulations mimic the physical movement of the atoms in a receptor−ligand complex within a certain time. Our results suggest that MD simulation is an effective supplementary procedure to the pharmacophore models and molecular docking methods.

Conformations Predicted by the Pharmacophore Model. The structures of the 15 potent inhibitors are illustrated as Figure 5. Six of the most potent compounds mapped with the pharmacophore model are shown in Supporting Information Figure S3. It is easy to see that the six compounds matched the pharmacophore model well.

Five out of six features of the derived pharmacophore model are located on the left side. These features contain two unified HydlAro (hydrophobic centroid or aromatic center, green) properties, a unified AroIPiR (aromatic center or Pi ring center, dark green) property, an Acc (H-bond acceptor, purple) property, and an Acc2 (H-bond acceptor projection, blue) property. For each of the six most potent compounds, a small part of the molecule matched all of the five features, as shown in Supporting Information Figure S3 marked by the dashed box, while a large part matches the remaining one. This phenomenon suggests that these five features play important roles in the high-affinity interactions between these inhibitors and their target PDE4D.

Binding Modes after 8 ns MD Simulations. To understand the structural basis for the binding of these hits to PDE4D's binding site, we scrutinized the binding poses by means of MD simulations. Binding modes of the six most potent compounds after 8 ns MD simulations are shown as Figure 6. The best molecule in picture 1 (Figure 6) shows common interactions with the invariant Gln369 and Phe372 on the left side, while other molecules in pictures 2, 3, 4, and 6 show similar binding modes. Comparing these structures, we can see that all of them have the similar catechol scaffold found in roflumilast, which plays a key role in the high-affinity interactions between inhibitors and PDE4D. In addition, the right side of the small molecules mainly forms hydrophobic interactions and van der Waals interactions with the binding pocket of PDE4D.

The structure as shown in picture 5, whose left side is a scaffold of quinoline, is quite different from the other five structures. Quinoline is nothing like a catechol analogue, but its nitrogen can make specific H-bond interactions with Gln369, while the aromatic ring of quinoline can form $\pi-\pi$ stacking interaction with Phe372. The binding modes of the six compounds indicate that $\pi-\pi$ stacking and H-bond interactions with Phe372 and Gln369 are very important binding features to account for their strong inhibitory affinities.

Except the binding features that we can figure out readily, more detailed interactions between PDE4D and hits were analyzed by using the protein−ligand interaction fingerprints (PLIF) module in MOE 2008.10.[24,25] The result of our PLIF analysis of the fifteen potent compounds is shown as Figure 7. Almost every compound makes intermolecular interactions with the two residues (Phe372 and Gln369), and most of them form two H-bonds with Gln369. In addition, most of them involve interactions with Met273 and Ile336. These results suggest that Gln369, Phe372, Met273, and Ile336 are the key residues for the interactions between PDE4D and ligands and should be considered carefully in the structure-based design of PDE4D inhibitors.

4. CONCLUSIONS

In this study, an integrated computational procedure consisted of pharmacophore, molecular docking, MD simulations, ΔG_{pred} calculations, and final bioassay validation was adopted to screen PDE4D inhibitors against the SPECS database. After 8 ns MD simulation for each of the 224 PDE4D−inhibitor complexes, 29 compounds with relatively negative ΔG_{pred} and appropriate binding patterns were selected for bioassay. Fifteen of the 29 tested compounds were found as potent inhibitors via PDE4D bioassay, indicating the high hit rate of this MD-augmented approach. The most potent compound has an IC_{50} value of 1.9 μM. Thus, we can conclude that the MD simulations can enhance the hit rate significantly. This approach provides an effective and efficient screening workflow for the discovery of PDE4D inhibitors. The MD-augmented virtual screening strategy employed here could in principle be applied to the identification of competitive inhibitors of other PDEs.

Besides the interactions with the invariant residues Phe372 and Gln369, MOE PLIF further identified that most of the potent compounds also involve interactions with Met273 and Ile336. Thus, these four residues should be considered collectively carefully in the structure-based design of PDE4D inhibitors.

■ ASSOCIATED CONTENT

Ⓢ Supporting Information

Thirty PDE4D inhibitors selected from the Binding Database, RMSD curve of the simulated PDE4D−roflumilast complex, and six of the most potent compounds mapping with the pharmacophore model. This material is available free of charge via the Internet at http://pubs.acs.org.

■ AUTHOR INFORMATION

Corresponding Author

*Tel.: 86-20-39943031. E-mail: luohb77@mail.sysu.edu.cn.

Author Contributions

⊥Z.L. and Y.-H.C.: These authors contributed equally.

Notes

The authors declare no competing financial interest.

■ ACKNOWLEDGMENTS

We cordially thank Prof. H. Ke in the Department of Biochemistry and Biophysics at the University of North Carolina, Chapel Hill, for his suggestion and help for molecular cloning, expression, purification, and enzymatic assay of PDE4D2 and the High Performance Supercomputer Center at Sun Yat-Sen University. This work is supported by the Natural Science Foundation of China (21103234), Guangdong Natural Science Foundation (S2011030003190), Guangdong Science Foundation (2012A080201007), Science Foundation of Department of Education in Guangdong Province (CXZD1006), Fundamental Research Funds for the Central Universities (11ykzd05), and Research Funds (2012) from Advanced Technology Institute.

REFERENCES

(1) Cho-Chung, Y. S.; Clair, T. The regulatory subunit of cAMP-dependent protein kinase as a target for chemotherapy of cancer and other cellular dysfunctional-related diseases. *Pharmacol. Ther.* **1993**, *60* (2), 265−288.

(2) Edwards, H. V.; Christian, F.; Baillie, G. S. cAMP: Novel concepts in compartmentalised signalling. *Semin. Cell Dev. Biol.* **2012**, *23* (2), 181−190.

(3) Jeon, Y. H.; Heo, Y. S.; Kim, C. M.; Hyun, Y. L.; Lee, T. G.; Ro, S.; Cho, J. M. Phosphodiesterase: Overview of protein structures, potential therapeutic applications and recent progress in drug development. *Cell. Mol. Life Sci.* **2005**, *62* (11), 1198−1220.

(4) Bender, A. T.; Beavo, J. A. Cyclic nucleotide phosphodiesterases: Molecular regulation to clinical use. *Pharmacol. Rev.* **2006**, *58*, 488−520.

(5) Omori, K.; Kotera, J. Overview of PDEs and their regulation. *Circ. Res.* **2007**, *100*, 309−327.

(6) Zaccolo, M.; Movsesian, M. A. cAMP and cGMP signaling crosstalk: Role of phosphodiesterases and implications for cardiac pathophysiology. *Circ. Res.* **2007**, *100*, 1569−1578.

(7) Ke, H.; Wang, H. Crystal structures of phosphodiesterases and implications on substrate specificity and inhibitor selectivity. *Curr. Top. Med. Chem.* **2007**, *7*, 391−403.

(8) Hou, J.; Xu, J.; Liu, M.; Zhao, R.; Luo, H.-B.; Ke, H. Structural asymmetry of phosphodiesterase-9, potential protonation of a glutamic acid, and role of the invariant glutamine. *PLoS ONE* **2011**, *6*, e18092.

(9) Meng, F.; Hou, J.; Shao, Y. X.; Wu, P. Y.; Huang, M.; Zhu, X.; Cai, Y. H.; Li, Z.; Xu, J.; Liu, P. Q.; Luo, H.-B.; Wan, Y. Q.; Ke, H. Structure-based discovery of highly selective phosphodiesterase-9A inhibitors and implications for inhibitor design. *J. Med. Chem.* **2012**, *55* (19), 8549−8558.

(10) Chen, S. K.; Zhao, P.; Shao, Y. X.; Li, Z.; Zhang, C.; Liu, P. Q.; He, X.; Luo, H.-B.; Hu, X. Moracin M from *Morus alba L.* is a natural phosphodiesterase-4 inhibitor. *Bioorg. Med. Chem. Lett.* **2012**, *22* (9), 3261−3264.

(11) Houslay, M. D.; Schafer, P.; Zhang, K. Y. Keynote review: phosphodiesterase-4 as a therapeutic target. *Drug Discov. Today* **2005**, *10* (22), 1503−1519.

(12) Jeffery, P. Phosphodiesterase 4-selective inhibition: novel therapy for the inflammation of COPD. *Pulm. Pharmacol. Ther.* **2005**, *18* (1), 9−17.

(13) O'Donnell, J. M.; Zhang, H. T. Antidepressant effects of inhibitors of cAMP phosphodiesterase (PDE4). *Trends Pharmacol. Sci.* **2004**, *25* (3), 158−163.

(14) Page, C. P.; Spina, D. Selective PDE inhibitors as novel treatments for respiratory diseases. *Curr. Opin. Pharmacol.* **2012**, *12* (3), 275−286.

(15) Spina, D. The potential of PDE4 inhibitors in respiratory disease. *Curr. Drug Targets Inflamm. Allergy* **2004**, *3* (3), 231−236.

(16) O'Byrne, P. M.; Gauvreau, G. Phosphodiesterase-4 inhibition in COPD. *Lancet* **2009**, *374* (9691), 665−667.

(17) Park, S. J.; Ahmad, F.; Philp, A.; Baar, K.; Williams, T.; Luo, H.-B; Ke, H.; Rehmann, H.; Taussig, R.; Brown, A. L.; Kim, M. K.; Beaven, M. A.; Burgin, A. B.; Manganiello, V.; Chung, J. H. Resveratrol ameliorates aging-related metabolic phenotypes by inhibiting cAMP phosphodiesterases. *Cell* **2012**, *148* (3), 421−433.

(18) Gretarsdottir, S.; Thorleifsson, G.; Reynisdottir, S. T.; Manolescu, A.; Jonsdottir, S.; Jonsdottir, T.; Gudmundsdottir, T.; Bjarnadottir, S. M.; Einarsson, O. B.; Gudjonsdottir, H. M.; Hawkins, M.; Gudmundsson, G.; Gudmundsdottir, H.; Andrason, H.; Gudmundsdottir, A. S.; Sigurdardottir, M.; Chou, T. T.; Nahmias, J.; Goss, S.; Sveinbjornsdottir, S.; Valdimarsson, E. M.; Jakobsson, F.; Agnarsson, U.; Gudnason, V.; Thorgeirsson, G.; Fingerle, J.; Gurney, M.; Gudbjartsson, D.; Frigge, M. L.; Kong, A.; Stefansson, K.; Gulcher, J. R. The gene encoding phosphodiesterase 4D confers risk of ischemic stroke. *Nat. Genet.* **2003**, *35* (2), 131−138.

(19) Bevan, S.; Porteous, L.; Sitzer, M.; Markus, H. S. Phosphodiesterase 4D gene, ischemic stroke, and asymptomatic carotid atherosclerosis. *Stroke* **2005**, *36* (5), 949−953.

(20) Saleheen, D.; Bukhari, S.; Haider, S. R.; Nazir, A.; Khanum, S.; Shafqat, S.; Anis, M. K.; Frossard, P. Association of phosphodiesterase 4D gene with ischemic stroke in a Pakistani population. *Stroke* **2005**, *36* (10), 2275−2277.

(21) Munshi, A.; Roy, S.; Thangaraj, K.; Kaul, S.; Babu, M. S.; Jyothy, A. Association of SNP41, SNP56 and a novel SNP in PDE4D gene with stroke and its subtypes. *Gene* **2012**, *506*, 31−35.

(22) Chen, K. C.; Chang, K. W.; Chen, H. Y.; Chen, C. Y. Traditional Chinese medicine, a solution for reducing dual stroke risk factors at once? *Mol. Biosyst.* **2011**, *7* (9), 2711−2719.

(23) Chen, Z.; Tian, G.; Wang, Z.; Jiang, H.; Shen, J.; Zhu, W. Multiple pharmacophore models combined with molecular docking: a reliable way for efficiently identifying novel PDE4 inhibitors with high structural diversity. *J. Chem. Inf. Model.* **2010**, *50* (4), 615−625.

(24) *MOE 2008.10*, Chemical Computing Group Inc., Montreal, Quebec, Canada, 2008.

(25) Mize, C. D.; Abbott, A. M.; Gacasan, S. B.; Parrill, A. L.; Baker, D. L. Ligand-based autotaxin pharmacophore models reflect structure-based docking results. *J. Mol. Graph. Model.* **2011**, *31*, 76−86.

(26) Card, G. L.; England, B. P.; Suzuki, Y.; Fong, D.; Powell, B.; Lee, B.; Luu, C.; Tabrizizad, M.; Gillette, S.; Ibrahim, P. N.; Artis, D. R.; Bollag, G.; Milburn, M. V.; Kim, S. H.; Schlessinger, J.; Zhang, K. Y. Structural basis for the activity of drugs that inhibit phosphodiesterases. *Structure* **2004**, *12* (12), 2233−2247.

(27) Burgin, A. B.; Magnusson, O. T.; Singh, J.; Witte, P.; Staker, B. L.; Bjornsson, J. M.; Thorsteinsdottir, M.; Hrafnsdottir, S.; Hagen, T.; Kiselyov, A. S.; Stewart, L. J.; Gurney, M. E. Design of phosphodiesterase 4D (PDE4D) allosteric modulators for enhancing cognition with improved safety. *Nat. Biotechnol.* **2010**, *28* (1), 63−70.

(28) (a) Chen, X.; Lin, Y.; Liu, M.; Gilson, M. K. The Binding Database: Data management and interface design. *Bioinformatics* **2002**, *18* (1), 130−139. (b) Liu, T.; Lin, Y.; Wen, X.; Jorissen, R. N.; Gilson, M. K. BindingDB: A web-accessible database of experimentally determined protein-ligand binding affinities. *Nucleic Acids Res.* **2007**, *35*, D198−D201.

(29) Huang, N.; Shoichet, B. K.; Irwin, J. J. Benchmarking sets for molecular docking. *J. Med. Chem.* **2006**, *49* (23), 6789−6801.

(30) Vadivelan, S.; Sinha, B. N.; Irudayam, S. J.; Jagarlapudi, S. A. Virtual screening studies to design potent CDK2-cyclin A inhibitors. *J. Chem. Inf. Model.* **2007**, *47*, 1526−35.

(31) Boppana, K.; Dubey, P. K.; Jagarlapudi, S. A.; Vadivelan, S.; Rambabu, G. Knowledge based identification of MAO-B selective inhibitors using pharmacophore and structure based virtual screening models. *Eur. J. Med. Chem.* **2009**, *44*, 3584−90.

(32) Shih, K. C.; Lin, C. Y.; Zhou, J.; Chi, H. C.; Chen, T. S.; Wang, C. C.; Tseng, H. W.; Tang, C. Y. Development of novel 3D-QSAR combination approach for screening and optimizing B-Raf inhibitors *in silico*. *J. Chem. Inf. Model.* **2011**, *51* (2), 398−407.

(33) Wu, G.; Robertson, D. H.; Brooks, C. R.; Vieth, M. Detailed analysis of grid-based molecular docking: A case study of CDOCKER-A CHARMm-based MD docking algorithm. *J. Comput. Chem.* **2003**, *24* (13), 1549−1562.

(34) Case, D. A.; Darden, T. A.; Cheatham, T. E. III; Simmerling, C. L.; Wang, J.; Duke, R. E.; Luo, R.; Walker, R. C.; Zhang, W.; Merz, K. M.; Roberts, B. P.; Hayik, S.; Roitberg, A.; Seabra, G.; Swails, J.; Götz, A. W.; Kolossváry, I.; Wong, K. F.; Paesani, F.; Vanicek, J.; Wolf, R. M.; Liu, J.; Wu, X.; Brozell, S. R.; Steinbrecher, T.; Gohlke, H.; Cai, Q.; Ye, X.; Wang, J.; Hsieh, M. J.; Cui, G.; Roe, D. R.; Mathews, D. H.; Seetin, M. G.; Salomon-Ferrer, R.; Sagui, C.; Babin, V.; Luchko, T.; Gusarov, S.; Kovalenko, A.; Kollman, P. A. *AMBER 10*; University of California, San Francisco, 2008.

(35) Frisch, M. J.; Trucks, G. W.; Schlegel, H. B.; et al. *Gaussian 03*, Revision E.01; Gaussian, Inc.: Pittsburgh PA, 2004.

(36) Wang, J.; Wang, W.; Kollman, P. A.; Case, D. A. Automatic atom type and bond type perception in molecular mechanical calculations. *J. Mol. Graph. Model.* **2006**, *25* (2), 247−260.

(37) Stote, R. H.; Karplus, M. Zinc binding in proteins and solution: a simple but accurate nonbonded representation. *Proteins* **1995**, *23* (1), 12−31.

(38) Xiong, Y.; Lu, H. T.; Li, Y.; Yang, G. F.; Zhan, C. G. Characterization of a catalytic ligand bridging metal ions in phosphodiesterases 4 and 5 by molecular dynamics simulations and hybrid quantum mechanical/molecular mechanical calculations. *Biophys. J.* **2006**, *91* (5), 1858−1867.
(39) Shuichi, M.; Kollman, P. A. Settle: An analytical version of the SHAKE and RATTLE algorithm for rigid water models. *J. Comput. Chem.* **1992**, *8* (13), 952−962.
(40) Massova, I.; Kollman, P. A. Combined molecular mechanical and continuum solvent approach (MM-PBSA/GBSA) to predict ligand binding. *Perspect Drug Discov. Des.* **2000**, *1* (18), 113−135.
(41) Hou, T. J.; Wang, J.; Li, Y.; Wang, W. Assessing the performance of the MM/PBSA and MM/GBSA methods. 1. The accuracy of binding free energy calculations based on molecular dynamics simulations. *J. Chem. Inf. Model.* **2011**, *51* (1), 69−82.
(42) Liu, M.; Yuan, M.; Luo, M.; Bu, X.; Luo, H.-B.; Hu, X. Binding of curcumin with glyoxalase I: Molecular docking, molecular dynamics simulations, and kinetics analysis. *Biophys. Chem.* **2010**, *147*, 28−34.
(43) He, L.; He, F.; Bi, H.; Li, J.; Zeng, S.; Luo, H.-B.; Huang, M. Isoform-selective inhibition of chrysin towards human cytochrome P450 1A2. Kinetics analysis, molecular docking, and molecular dynamics simulations. *Bioorg. Med. Chem. Lett.* **2010**, *20*, 6008−6012.
(44) Jain, A. N. Surflex-Dock 2.1: Robust performance from ligand energetic modeling, ring flexibility, and knowledge-based search. *J. Comput.-Aided. Mol. Des.* **2007**, *21*, 281−306.